THE JOURNAL OF PHYSICAL CHEMISTRY Letters

pubs.acs.org/JPCL Letter

Experimental and Simulation Insights into Local Structure and Luminescence Evolution in Eu^{3+}-Doped Nanocrystals under High Pressure

Sheng Mei, Yu Guo, Xiaohuan Lin, Hao Dong, Ling-Dong Sun,* Kuo Li,* and Chun-Hua Yan*

Cite This: *J. Phys. Chem. Lett.* 2020, 11, 3515−3520 Read Online

ACCESS | Metrics & More | Article Recommendations | Supporting Information

ABSTRACT: Tremendous effort has been devoted to tailoring structure-correlated properties, especially for the luminescence of lanthanide nanocrystals (NCs). High pressure has been demonstrated as a decent way to tune the performance of lanthanide NCs; however, little attention has been paid to the local structure evolution accompanied by extreme compression and its effect on luminescence. Here, we tailor the local structure around lanthanide ions with pressure in β-$NaGdF_4$ NCs, in which Eu^{3+} ions were doped as optical probes for local structure for the sensitive electric dipole transition. As the pressure increases, the intensity ratio of the $^5D_0 \rightarrow {}^7F_2$ to $^5D_0 \rightarrow {}^7F_1$ transition decreases monotonically from 2.04 to 0.81, implying a higher local symmetry around Eu^{3+} ions from compression. *In situ* X-ray diffraction demonstrates that the sample maintains the hexagonal structure up to 33.5 GPa, and density functional theory calculations reveal the tendency of the local structure to vary under high pressure.

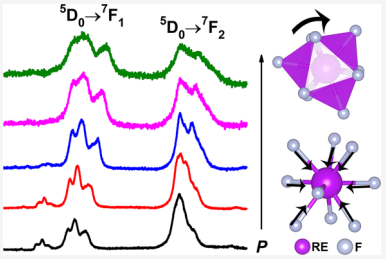

Lanthanide-doped nanophosphors have attracted extensive attention in recent years due to their high photostability and large Stokes/anti-Stokes shifts, as well as tunable emission colors and luminescence lifetimes.[1−3] Typically emitters, lanthanide ions are doped in a host as a luminescent material. Among various types of host materials, sodium rare earth (RE) fluorides, namely $NaREF_4$, which benefit from a low phonon energy and a high chemical stability, have been reported as some of the most efficient host matrices, especially for upconversion emissions.[4,5] Intriguingly, hexagonal phase β-$NaREF_4$ nanocrystals (NCs) accommodate lower local site symmetry around doping ions,[6] which effectively relieve the parity-forbidden 4f−4f intraconfigurational transitions and offer a luminescence intensity that is an order of magnitude higher than those of the cubic phase counterparts.[7−9]

To further free lanthanide-doped NCs from the parity-forbidden rule, tailoring the local structure around luminescent centers has proven to be effective. Several strategies have been developed to tailor the local structure, including doping optically inert cations,[10−12] introducing an external electric field,[13] modulating the composition,[14] etc. These strategies not only lead to enhancement of luminescence but also obviously alter the emission selectivity. However, the aforementioned methods either require massive trials of synthesis or cater to only specific systems. Straightforward methods are needed to tailor the local crystal field of host materials efficiently.

Pressure has been reported to be an effective way to tune the structure and properties of various materials.[15] Under high pressure, the distance between neighboring atoms or molecules will be shortened, which could further induce the evolution of electron correlation and electron−phonon interaction.[16−18] Recently, a few studies have examined the properties of lanthanide-doped $NaREF_4$-based NCs under high pressure.[19−21] Among them, luminescent characteristics such as the emission intensity, spectral profile, and emission lifetime have been investigated. However, most previous reports are based on upconversion systems, which require the co-doping of sensitizers and activators, and it is difficult to elucidate the relationship of local structure and luminescent behaviors as the energy transfer route is variable. By contrast, Eu^{3+} ions have long been regarded as a good optical probe for local structure. The $^5D_0 \rightarrow {}^7F_1$ transition is a primarily magnetic dipole one and independent of crystal field; the $^5D_0 \rightarrow {}^7F_2$ transition is essentially purely electric dipole in nature, and its intensity is sensitive to the local crystal field.[22,23] Furthermore, the intensity ratio of the $^5D_0 \rightarrow {}^7F_2$ to $^5D_0 \rightarrow {}^7F_1$ transition could well reflect the local symmetry difference.[24−26] Using Eu^{3+} ions to probe the local structure evolution would deepen our understanding of the pressure-dependent emission behaviors of $NaREF_4$ NCs.

In this work, we investigated the *in situ* photoluminescence (PL) evolution of β-$NaGdF_4$:Eu^{3+} NCs under high pressure. Eu^{3+} ions acted as a probe to indicate the tendency of local

Received: March 21, 2020
Accepted: April 15, 2020
Published: April 15, 2020

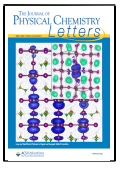

symmetry during the compression−decompression cycle. Unlike the evolution trend reported in YF_3 NCs,[26] YPO_4 NCs,[27] and other Eu^{3+}-doped materials,[25,28] the higher pressure led a higher local symmetry around Eu^{3+} ions in β-$NaGdF_4$:Eu^{3+} NCs. *In situ* angle dispersive synchrotron X-ray diffraction was conducted to investigate the structure evolution of β-$NaGdF_4$:Eu^{3+} NCs. No obvious phase change was observed throughout the process. *In situ* PL spectra of β-$NaGdF_4$:Eu^{3+} NCs of various sizes under high pressure revealed that the crystal size did not play a significant role in the local structure evolution. Density functional theory (DFT) calculations indicate that the lateral local symmetry of rare earth ions increases while the vertical local symmetry decreases with the increase in pressure.

β-$NaGdF_4$:Eu^{3+} NCs were synthesized with a modified thermal decomposition method.[29] The TEM image in Figure 1a reveals the uniformity of the as-synthesized samples. The

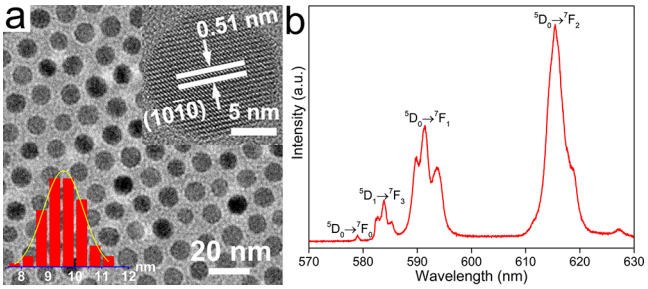

Figure 1. (a) TEM image, HRTEM image (top inset), and size distribution (bottom inset) of β-$NaGdF_4$:Eu^{3+} NCs. (b) Emission spectrum of β-$NaGdF_4$:Eu^{3+} NCs under ambient conditions.

high-resolution TEM (HRTEM) image (top inset of Figure 1a) shows a single-crystal nature with a lattice spacing of 0.51 nm, which corresponds to the (10$\bar{1}$0) plane of hexagonal $NaGdF_4$. The mean particle size of β-$NaGdF_4$:Eu^{3+} NCs is 9.6 ± 0.5 nm (bottom inset of Figure 1a), and the XRD pattern of the NCs corresponds well to the standard pattern of hexagonal $NaGdF_4$ (Figure S1). Figure 1b illustrates the PL spectrum of β-$NaGdF_4$:Eu^{3+} NCs under ambient conditions, which shows typical emission bands of Eu^{3+} ions, including $^5D_0 \rightarrow {}^7F_0$, $^7F_1$, $^7F_2$, and $^5D_1 \rightarrow {}^7F_3$. The appearance of strictly forbidden $^5D_0 \rightarrow {}^7F_0$ emission at 579.0 nm at room temperature demonstrates a lower site symmetry for Eu^{3+} ions.[30] The $^5D_1 \rightarrow {}^7F_3$ transition shows three emission peaks, centered at 582.7, 583.9, and 585.3 nm. The $^5D_0 \rightarrow {}^7F_1$ transition also displays three peaks at 589.9, 591.4, and 593.6 nm. The crystal-field splitting of emission peaks corresponds well with that of β-$NaYF_4$:Eu^{3+} NCs,[6] implying similar site symmetry broken in β-$NaGdF_4$. Intriguingly, the electric dipole emission of the $^5D_0 \rightarrow {}^7F_2$ transition (centered at 615.5 nm) is more intense than that of the magnetic dipole emission of the $^5D_0 \rightarrow {}^7F_1$ transition, which further confirms a lower local symmetry of β-$NaGdF_4$ NCs.

Next, we introduce the as-prepared NCs into a diamond anvil cell (DAC) to examine the luminescence under high pressure. Figure 2a demonstrates the evolution of PL spectra with the pressure increasing from 0.7 to 30.2 GPa. The signal-to-noise ratio decreased significantly as the pressure exceeded 15 GPa, which implied a decreased overall PL intensity. This arises from exacerbated nonradiative relaxation under high pressure, which could be caused by both the formation of

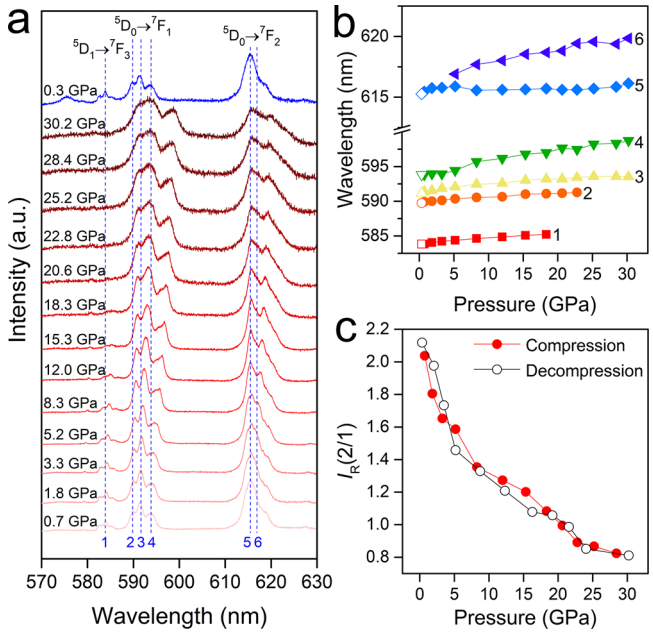

Figure 2. (a) Normalized emission spectra of β-$NaGdF_4$:Eu^{3+} NCs with a 0.7 GPa−30.2 GPa−0.3 GPa compression−decompression cycle. (b) Pressure-induced shifts of emission peaks denoted in panel a with compression (filled) and decompression (0.3 GPa, empty). (c) Variation of intensity ratios $I_R(2/1)$ of β-$NaGdF_4$:Eu^{3+} NCs during the compression (filled circles) and decompression (empty circles) cycle.

defects and the increased phonon energy of the host matrix.[19] Above 18.3 GPa, the $^5D_1 \rightarrow {}^7F_3$ transition became indistinct, and the weak emission of the $^5D_0 \rightarrow {}^7F_0$ transition also became hard to identify. However, the main two transitions, $^5D_0 \rightarrow {}^7F_1$ and $^5D_0 \rightarrow {}^7F_2$, maintained decent emission intensity under high pressure. Notably, the $^5D_1 \rightarrow {}^7F_3$, $^5D_0 \rightarrow {}^7F_1$, and $^5D_0 \rightarrow {}^7F_2$ transitions could revert to their original shape upon release of pressure, while the $^5D_0 \rightarrow {}^7F_0$ emission remained indistinguishable even when the pressure was decreased to 0.3 GPa (Figure S2).

Pressure-induced peak shifts are also observed during the compression process. In general, the emissions slightly red-shift with pressure but to different extents (Figure 2b). We monitor this tendency of a few main emission peaks as denoted in Figure 2a. It clearly indicates that peak 4 from the $^5D_0 \rightarrow {}^7F_1$ transition shows the largest shift, i.e., from 593.8 to 598.8 nm. By contrast, the initially most intense peak 5 from the $^5D_0 \rightarrow {}^7F_2$ transition shows only a small shift from 615.5 to 616.1 nm. As a result, these two transitions are getting closer together with the compression. Furthermore, most of the emission peaks become broader and less intense as the pressure increases. For example, three obvious peaks (peaks 2−4) could be resolved from the $^5D_0 \rightarrow {}^7F_1$ transition under ambient conditions, while peaks 2 and 3 almost merged into a broader peak at 30.2 GPa. Meanwhile, the sharp peak of the $^5D_0 \rightarrow {}^7F_2$ transition split into two under high pressure. A similar peak shift and broadening phenomenon has also been reported in other lanthanide-doped systems.[31,32] These changes can be attributed to prominent splitting of both excited and ground state levels under high pressure, which not only narrows the energy difference between excited and ground states but also expands the subenergy levels simultaneously, giving rise to red-shifted broadened peaks.[31]

https://dx.doi.org/10.1021/acs.jpclett.0c00895
J. Phys. Chem. Lett. 2020, 11, 3515−3520

To evaluate the local symmetry evolution around Eu^{3+} ions, we calculate the PL intensity ratio of the $^5D_0 \rightarrow {}^7F_2$ to $^5D_0 \rightarrow {}^7F_1$ transition, $I_R(2/1)$, which is strongly correlated with the asymmetry and used as an indicator to elucidate the evolution tendency. Figure 2c shows the variation of $I_R(2/1)$ during a compression−decompression cycle. Initially, the value of $I_R(2/1)$ was 2.04, a pretty high value compared to the previously reported value of ∼0.3 for YF_3:Eu^{3+} NCs;[26] this also confirmed that $NaGdF_4$ is known as one of the most efficient host matrices for luminescent studies. However, an increase in pressure leads to a monotonic decrease in $I_R(2/1)$, which declines to 0.81 at 30.2 GPa. The decreased value of $I_R(2/1)$ with pressure indicates an increased local symmetry around Eu^{3+} ions. Furthermore, decompression results in a change in the opposite trend and a bit larger $I_R(2/1)$ after a compression−decompression cycle.

Aiming to monitor the crystal structure evolution under varied pressures, we performed *in situ* synchrotron XRD measurements. Figure 3a displays typical diffraction patterns

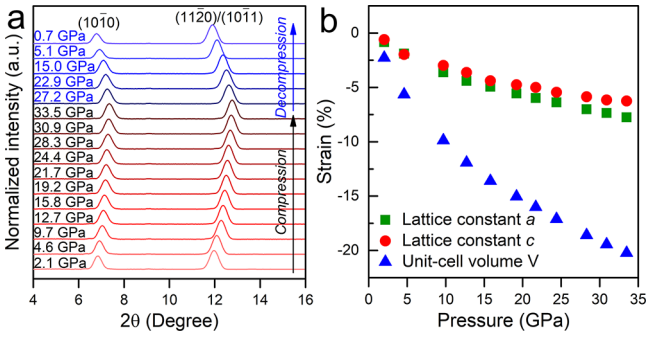

Figure 3. (a) XRD patterns (λ = 0.6199 Å) of β-$NaGdF_4$:Eu^{3+} NCs at different pressures. (b) High-pressure evolution of lattice parameters and unit cell volume (defined relative to the parameters at 0.7 GPa).

throughout the compression−decompression cycle. Two diffraction peaks can be observed, which correspond well to the (10$\bar{1}$0) and (11$\bar{2}$0)/(10$\bar{1}$1) facets of β-$NaGdF_4$. It is worth noting that the small interplanar spacing discrepancy between the (11$\bar{2}$0) and (10$\bar{1}$1) facets combined with a smaller particle size leads to indistinguishable diffraction peaks. A striking shift of the diffraction toward larger 2θ angles could be observed due to lattice contraction under increasing pressure, and the diffraction peaks revert to their initial values upon decompression. No new peaks emerge or disappear throughout the cycle, indicating no sign of phase transformation. The absence of phase transition is consistent with previous investigations of β-$NaYF_4$ bulk materials and β-$NaYF_4$ NCs.[19,33] We further calculate the evolution of lattice parameters throughout the cycle by performing Rietveld refinements (Table S1 and Figure 3b). Under the maximum pressure we applied (33.5 GPa), a and c shrank by 7.8% and 6.2%, respectively, leading to a reduction in unit cell volume of approximately 20.2%. The P−V data are fitted on the basis of the third-order Brich−Murnaghan equation of state (see details in Figure S3). These drastic changes in lattice parameters further reflect the structural stability of β-$NaREF_4$.

On the basis of the paradigm of 10 nm NCs, we extended the pressure-induced local structure evolution to β-$NaGdF_4$:Eu^{3+} NCs of varied sizes. Crystal size has been demonstrated to be a crucial factor in pressure-induced structure and property evolution in various materials, including TiO_2 NCs,[34] Y_2O_3 NCs,[35] and PbTe NCs,[36] and the high-pressure behavior of nanoparticles could substantially vary even with a small size difference. To study the effect of particle size, we synthesized ∼40, ∼250, and ∼500 nm β-$NaGdF_4$:Eu^{3+} NCs. Interestingly, *in situ* PL spectra of these samples showed a similar evolution trend throughout the compression−decompression cycle (Figures S4−S6). The value of $I_R(2/1)$ experienced a monotonic decrease during the compression process, and it bounced back to a slightly larger one after decompression (Figure S7). These results corroborate that the particle size does not play a decisive role, and the local structure evolution of β-$NaGdF_4$ NCs under high pressure is independent of size and happens intrinsically. However, TEM images of different samples after the compression−decompression cycle did show a substantial distinction. The 10 and 40 nm NCs, which were prepared through a thermolysis method, maintained their morphology after the pressure cycle (Figures S8 and S9), while larger NCs prepared with the hydrothermal method formed aggregates of several micrometers (Figures S10 and S11). The difference in morphology evolution under pressure could arise from crystallization and surface capping ligands for NCs prepared via the thermolysis method.

DFT calculations are performed for the crystal structures under pressure to further unravel the evolution of local structure in β-$NaGdF_4$:Eu^{3+} NCs. The unit cell we construct has a formula of $Na_{18}Gd_{17}Eu_1F_{72}$ (Figure 4a), in which the doping ratio of the Eu^{3+} ion is 5.5%, close to the experimental value of 5%. The lattice parameters derived from *in situ* XRD are used as inputs to build and optimize the unit cells under different pressures. Both Eu^{3+} ions and Gd^{3+} ions are coordinated by nine F^- ions in a configuration close to a tricapped trigonal prism. As shown in Figure 4b, the top and bottom surfaces of the trigonal prism do not coincide with each other under ambient conditions, and an intersection angle is used to disclose the configuration of these two surfaces. With an increase in pressure from 0.7 to 33.5 GPa, the intersection angle decreases from 6.39° to 0.72° (Figure 4c and Table S2), indicating a gradual coincidence of these two surfaces that as a result leads to higher lateral symmetry. On the other hand, the RE−F bond length also decreases gradually with an increase in pressure due to lattice contraction (Figure 4c), and compared to the similar RE−F bond lengths under ambient conditions, those pointing to the two opposite top and bottom surfaces and the three caps turn out to have varied bond lengths under higher pressures, as can be seen from the diverse values in Table S2 and the increased variances in Figure S12, suggesting the decreased local symmetry along the c axis. The increased lateral local symmetry and decreased vertical local symmetry are in line with the additional lateral compression with pressures (Figure 3b). In particular, the binding energies are calculated to depict the interaction strength of the atoms within the structures, which turn out to increase generally along with the increase in pressure (Figure S13). Thus, the overall binding strength of the crystal increases with pressure, which helps to explain the continued variation of the local structure instead of the phase transition under high-pressure conditions.

In conclusion, we investigated the optical properties and local structure evolution of β-$NaGdF_4$:Eu^{3+} NCs under high pressure. Exerting an increased pressure leads to a decreased PL intensity, as well as the red-shift and broadening of emission peaks. Significantly, the PL intensity ratio of the $^5D_0$

https://dx.doi.org/10.1021/acs.jpclett.0c00895
J. Phys. Chem. Lett. 2020, 11, 3515−3520

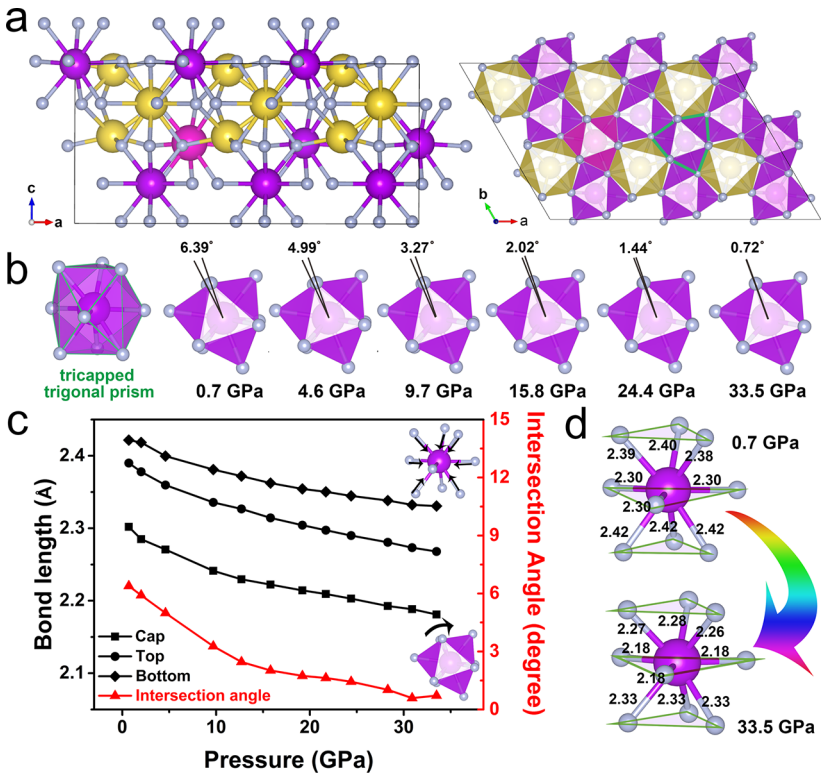

Figure 4. (a) Side view and top view of the Eu-doped $NaGdF_4$ unit cell under ambient conditions. The green lines highlight the selected Gd ion for the discussion of local symmetry. (b) High-pressure evolution of the selected Gd ion with a tricapped trigonal prism configuration. The black lines indicate the intersection angle of the top and bottom triangle surfaces of the trigonal prisms. (c) Variation of the average Gd−F bond length pointing to the top and bottom surfaces and three caps (black) and the intersection angle (red) with applied pressure. (d) Gd−F bond lengths at 0.7 and 33.5 GPa. Na (gold spheres), Gd (purple spheres), Eu (pink spheres), and F (gray spheres) atoms are shown.

$\rightarrow {}^7F_2$ to ${}^5D_0 \rightarrow {}^7F_1$ transition monotonically decreases with an increase in pressure, indicating higher local symmetry around Eu^{3+} ions. Furthermore, $NaGdF_4$ NCs remain in the hexagonal phase up to 33.5 GPa, the highest pressure we used, even with an ∼20% reduction in unit cell volume. Releasing pressure to ambient conditions leads to the recovery of both the structure and PL properties. The local structure evolution under pressure follows a similar trend in samples of varied sizes, which appears to be an intrinsic structural characteristic of $NaGdF_4$. DFT calculations further indicate the different local symmetry evolution trends in the lateral and vertical directions. This study emphasizes the effect of high pressure on the local structure of β-$NaGdF_4$, which would further influence the luminescence of lanthanide materials. Meanwhile, β-$NaGdF_4$ NCs display a relatively high phase stability, which could be applied under extreme conditions. Moreover, this Eu^{3+} doping strategy together with DFT simulations presents a promising approach for monitoring the local structure evolution.

■ ASSOCIATED CONTENT

Supporting Information

The Supporting Information is available free of charge at https://pubs.acs.org/doi/10.1021/acs.jpclett.0c00895.

Materials and methods, *in situ* emission spectra during the compression−decompression cycle, TEM images before and after compression, refined lattice parameters, and binding energies from DFT calculations (PDF)

■ AUTHOR INFORMATION

Corresponding Authors

Ling-Dong Sun − *Beijing National Laboratory for Molecular Sciences, State Key Laboratory of Rare Earth Materials Chemistry and Applications, PKU-HKU Joint Laboratory in Rare Earth Materials and Bioinorganic Chemistry, College of Chemistry and Molecular Engineering, Peking University, Beijing 100871, China*; Email: sun@pku.edu.cn

Kuo Li − *Center for High Pressure Science and Technology Advanced Research, Beijing 100094, China*; orcid.org/0000-0002-4859-6099; Email: likuo@hpstar.ac.cn

Chun-Hua Yan − *Beijing National Laboratory for Molecular Sciences, State Key Laboratory of Rare Earth Materials Chemistry and Applications, PKU-HKU Joint Laboratory in Rare Earth Materials and Bioinorganic Chemistry, College of Chemistry and Molecular Engineering, Peking University, Beijing 100871, China; College of Chemistry and Chemical Engineering, Lanzhou University, Lanzhou 730000, China*; orcid.org/0000-0002-0581-2951; Email: yan@pku.edu.cn

Authors

Sheng Mei − *Beijing National Laboratory for Molecular Sciences, State Key Laboratory of Rare Earth Materials Chemistry and Applications, PKU-HKU Joint Laboratory in Rare Earth Materials and Bioinorganic Chemistry, College of Chemistry and Molecular Engineering, Peking University, Beijing 100871, China*

Yu Guo − *Beijing National Laboratory for Molecular Sciences, State Key Laboratory of Rare Earth Materials Chemistry and Applications, PKU-HKU Joint Laboratory in Rare Earth*

https://dx.doi.org/10.1021/acs.jpclett.0c00895
J. Phys. Chem. Lett. 2020, 11, 3515−3520

Materials and Bioinorganic Chemistry, College of Chemistry and Molecular Engineering, Peking University, Beijing 100871, China

Xiaohuan Lin − *Center for High Pressure Science and Technology Advanced Research, Beijing 100094, China*

Hao Dong − *Beijing National Laboratory for Molecular Sciences, State Key Laboratory of Rare Earth Materials Chemistry and Applications, PKU-HKU Joint Laboratory in Rare Earth Materials and Bioinorganic Chemistry, College of Chemistry and Molecular Engineering, Peking University, Beijing 100871, China*

Complete contact information is available at: https://pubs.acs.org/10.1021/acs.jpclett.0c00895

Notes

The authors declare no competing financial interest.

■ ACKNOWLEDGMENTS

This work was supported by the National Natural Science Foundation of China (21590791, 21771005, 21931001, 21425101, 21771011, and 21875006) and the Ministry of Science and Technology (MOST) of China (2017YFA0205101 and 2017YFA0205104). The DFT calculations were performed on the High-performance Computing Platform of PKU. The *in situ* angle dispersive XRD measurements were performed at beamline 4W2 of the Beijing Synchrotron Radiation Facility (BSRF).

■ REFERENCES

(1) Liu, Y.; Tu, D.; Zhu, H.; Chen, X. Lanthanide-Doped Luminescent Nanoprobes: Controlled Synthesis, Optical Spectroscopy, and Bioapplications. *Chem. Soc. Rev.* **2013**, *42*, 6924−6958.

(2) Gai, S.; Li, C.; Yang, P.; Lin, J. Recent Progress in Rare Earth Micro/Nanocrystals: Soft Chemical Synthesis, Luminescent Properties, and Biomedical Applications. *Chem. Rev.* **2014**, *114*, 2343−2389.

(3) Dong, H.; Du, S.-R.; Zheng, X.-Y.; Lyu, G.-M.; Sun, L.-D.; Li, L.-D.; Zhang, P.-Z.; Zhang, C.; Yan, C.-H. Lanthanide Nanoparticles: from Design toward Bioimaging and Therapy. *Chem. Rev.* **2015**, *115*, 10725−10815.

(4) Menyuk, N.; Dwight, K.; Pierce, J. W. $NaYF_4$:Yb,Er—an Efficient Upconversion Phosphor. *Appl. Phys. Lett.* **1972**, *21*, 159−161.

(5) Suyver, J. F.; Grimm, J.; Krämer, K. W.; Güdel, H. U. Highly Efficient Near-Infrared to Visible Up-Conversion Process in $NaYF_4$:Er^{3+},Yb^{3+}. *J. Lumin.* **2005**, *114*, 53−59.

(6) Tu, D.; Liu, Y.; Zhu, H.; Li, R.; Liu, L.; Chen, X. Breakdown of Crystallographic Site Symmetry in Lanthanide-Doped $NaYF_4$ Crystals. *Angew. Chem., Int. Ed.* **2013**, *52*, 1128−1133.

(7) Krämer, K. W.; Biner, D.; Frei, G.; Güdel, H. U.; Hehlen, M. P.; Lüthi, S. R. Hexagonal Sodium Yttrium Fluoride Based Green and Blue Emitting Upconversion Phosphors. *Chem. Mater.* **2004**, *16*, 1244−1251.

(8) Yi, G. S.; Chow, G. M. Synthesis of Hexagonal-Phase $NaYF_4$:Yb,Er and $NaYF_4$:Yb,Tm Nanocrystals with Efficient Up-Conversion Fluorescence. *Adv. Funct. Mater.* **2006**, *16*, 2324−2329.

(9) Wang, F.; Han, Y.; Lim, C. S.; Lu, Y.; Wang, J.; Xu, J.; Chen, H.; Zhang, C.; Hong, M.; Liu, X. Simultaneous Phase and Size Control of Upconversion Nanocrystals through Lanthanide Doping. *Nature* **2010**, *463*, 1061−1065.

(10) Chen, G.; Liu, H.; Liang, H.; Somesfalean, G.; Zhang, Z. Upconversion Emission Enhancement in Yb^{3+}/Er^{3+}-Codoped Y_2O_3 Nanocrystals by Tridoping with Li^+ Ions. *J. Phys. Chem. C* **2008**, *112*, 12030−12036.

(11) Lei, L.; Chen, D.; Xu, J.; Zhang, R.; Wang, Y. Highly Intensified Upconversion Luminescence of Ca^{2+}-doped Yb/Er: $NaGdF_4$ Nanocrystals Prepared by a Solvothermal Route. *Chem. - Asian J.* **2014**, *9*, 728−733.

(12) Wisser, M. D.; Fischer, S.; Maurer, P. C.; Bronstein, N. D.; Chu, S.; Alivisatos, A. P.; Salleo, A.; Dionne, J. A. Enhancing Quantum Yield via Local Symmetry Distortion in Lanthanide-Based Upconverting Nanoparticles. *ACS Photonics* **2016**, *3*, 1523−1530.

(13) Hao, J.; Zhang, Y.; Wei, X. Electric-Induced Enhancement and Modulation of Upconversion Photoluminescence in Epitaxial $BaTiO_3$:Yb/Er Thin Films. *Angew. Chem., Int. Ed.* **2011**, *50*, 6876−6880.

(14) Dong, H.; Sun, L.-D.; Wang, Y.-F.; Ke, J.; Si, R.; Xiao, J.-W.; Lyu, G.-M.; Shi, S.; Yan, C.-H. Efficient Tailoring of Upconversion Selectivity by Engineering Local Structure of Lanthanides in Na_xREF_{3+x} Nanocrystals. *J. Am. Chem. Soc.* **2015**, *137*, 6569−6576.

(15) Mao, H.-K.; Chen, B.; Chen, J.; Li, K.; Lin, J.-F.; Yang, W.; Zheng, H. Recent Advances in High-Pressure Science and Technology. *Matter Radiat. Extremes* **2016**, *1*, 59−75.

(16) Santra, B.; Klimeš, J.; Alfè, D.; Tkatchenko, A.; Slater, B.; Michaelides, A.; Car, R.; Scheffler, M. Hydrogen Bonds and Van Der Waals Forces in Ice at Ambient and High Pressures. *Phys. Rev. Lett.* **2011**, *107*, 185701.

(17) Yu, H.; Lao, W.; Wang, L.; Li, K.; Chen, Y. Pressure-Stabilized Tin Selenide Phase with an Unexpected Stoichiometry and a Predicted Superconducting State at Low Temperatures. *Phys. Rev. Lett.* **2017**, *118*, 137002.

(18) Wang, L.; Dong, X.; Wang, Y.; Zheng, H.; Li, K.; Peng, X.; Mao, H.-k.; Jin, C.; Meng, Y.; Huang, M.; Zhao, Z. Pressure-Induced Polymerization and Disproportionation of Li_2C_2 Accompanied with Irreversible Conductivity Enhancement. *J. Phys. Chem. Lett.* **2017**, *8*, 4241−4245.

(19) Wisser, M. D.; Chea, M.; Lin, Y.; Wu, D. M.; Mao, W. L.; Salleo, A.; Dionne, J. A. Strain-Induced Modification of Optical Selection Rules in Lanthanide-Based Upconverting Nanoparticles. *Nano Lett.* **2015**, *15*, 1891−1897.

(20) Lay, A.; Wang, D. S.; Wisser, M. D.; Mehlenbacher, R. D.; Lin, Y.; Goodman, M. B.; Mao, W. L.; Dionne, J. A. Upconverting Nanoparticles as Optical Sensors of Nano- to Micro-Newton Forces. *Nano Lett.* **2017**, *17*, 4172−4177.

(21) Lay, A.; Siefe, C.; Fischer, S.; Mehlenbacher, R. D.; Ke, F.; Mao, W. L.; Alivisatos, A. P.; Goodman, M. B.; Dionne, J. A. Bright, Mechanosensitive Upconversion with Cubic-Phase Heteroepitaxial Core−Shell Nanoparticles. *Nano Lett.* **2018**, *18*, 4454−4459.

(22) Kirby, A. F.; Foster, D.; Richardson, F. S. Comparison of $^7F_J \leftarrow {}^5D_0$ Emission Spectra for Eu(III) in Crystalline Environments of Octahedral, Near-Octahedral, and Trigonal Symmetry. *Chem. Phys. Lett.* **1983**, *95*, 507−512.

(23) Jia, C.-J.; Sun, L.-D.; Luo, F.; Jiang, X.-C.; Wei, L.-H.; Yan, C.-H. Structural Transformation Induced Improved Luminescent Properties for $LaVO_4$:Eu Nanocrystals. *Appl. Phys. Lett.* **2004**, *84*, 5305−5307.

(24) Chen, G.; Haire, R. G.; Peterson, J. R. Effect of Pressure on Amorphous $Eu(OH)_3$: a Luminescence Study. *J. Phys. Chem. Solids* **1995**, *56*, 1095−1100.

(25) Zhang, C. C.; Zhang, Z. M.; Dai, R. C.; Wang, Z. P.; Zhang, J. W.; Ding, Z. J. High-Pressure Raman and Luminescence Study on the Phase Transition of $GdVO_4$:Eu^{3+} Microcrystals. *J. Phys. Chem. C* **2010**, *114*, 18279−18282.

(26) Gong, C.; Li, Q.; Liu, R.; Hou, Y.; Wang, J.; Dong, X.; Liu, B.; Tan, X.; Liu, J.; Yang, K.; Zou, B.; Cui, T.; Liu, B. Structural Phase Transition and Photoluminescence Properties of YF_3:Eu^{3+} Nanocrystals under High Pressure. *J. Phys. Chem. C* **2014**, *118*, 22739−22745.

(27) Yuan, H.; Wang, K.; Li, S.; Tan, X.; Li, Q.; Yan, T.; Cheng, B.; Yang, K.; Liu, B.; Zou, G.; Zou, B. Direct Zircon-to-Scheelite Structural Transformation in YPO_4 and YPO_4:Eu^{3+} Nanoparticles Under High Pressure. *J. Phys. Chem. C* **2012**, *116*, 24837−24844.

(28) Zhao, Y.; Yang, W.; Li, N.; Li, Y.; Tang, R.; Li, H.; Zhu, H.; Zhu, P.; Wang, X. Pressure-enhanced Insulating State and Trigonal

Distortion Relaxation in Geometrically Frustrated Pyrochlore $Eu_2Sn_2O_7$. *J. Phys. Chem. C* **2016**, *120*, 9436−9442.
(29) Mai, H.-X.; Zhang, Y.-W.; Si, R.; Yan, Z.-G.; Sun, L.-d.; You, L.-P.; Yan, C.-H. High-Quality Sodium Rare-Earth Fluoride Nanocrystals: Controlled Synthesis and Optical Properties. *J. Am. Chem. Soc.* **2006**, *128*, 6426−6436.
(30) Ptacek, P.; Schäfer, H.; Kömpe, K.; Haase, M. Crystal Phase Control of Luminescing α-$NaGdF_4$:Eu^{3+} and β-$NaGdF_4$:Eu^{3+} Nanocrystals. *Adv. Funct. Mater.* **2007**, *17*, 3843−3848.
(31) Renero-Lecuna, C.; Martín-Rodríguez, R.; Valiente, R.; González, J.; Rodríguez, F.; Krämer, K. W.; Güdel, H. U. Origin of the High Upconversion Green Luminescence Efficiency in β-$NaYF_4$:2%Er^{3+},20%Yb^{3+}. *Chem. Mater.* **2011**, *23*, 3442−3448.
(32) Runowski, M.; Shyichuk, A.; Tymiński, A.; Grzyb, T.; Lavín, V.; Lis, S. Multifunctional Optical Sensors for Nanomanometry and Nanothermometry: High-Pressure and High-Temperature Upconversion Luminescence of Lanthanide-Doped Phosphates—$LaPO_4$/YPO_4:Yb^{3+}−Tm^{3+}. *ACS Appl. Mater. Interfaces* **2018**, *10*, 17269−17279.
(33) Grzechnik, A.; Bouvier, P.; Mezouar, M.; Mathews, M. D.; Tyagi, A. K.; Köhler, J. Hexagonal $Na_{1.5}Y_{1.5}F_6$ at High Pressures. *J. Solid State Chem.* **2002**, *165*, 159−164.
(34) Swamy, V.; Kuznetsov, A.; Dubrovinsky, L. S.; McMillan, P. F.; Prakapenka, V. B.; Shen, G.; Muddle, B. C. Size-Dependent Pressure-Induced Amorphization in Nanoscale TiO_2. *Phys. Rev. Lett.* **2006**, *96*, 135702.
(35) Wang, L.; Yang, W.; Ding, Y.; Ren, Y.; Xiao, S.; Liu, B.; Sinogeikin, S. V.; Meng, Y.; Gosztola, D. J.; Shen, G.; Hemley, R. J.; Mao, W. L.; Mao, H.-K. Size-Dependent Amorphization of Nanoscale Y_2O_3 at High Pressure. *Phys. Rev. Lett.* **2010**, *105*, 095701.
(36) Quan, Z.; Wang, Y.; Bae, I.-T.; Loc, W. S.; Wang, C.; Wang, Z.; Fang, J. Reversal of Hall−Petch Effect in Structural Stability of PbTe Nanocrystals and Associated Variation of Phase Transformation. *Nano Lett.* **2011**, *11*, 5531−5536.

https://dx.doi.org/10.1021/acs.jpclett.0c00895
J. Phys. Chem. Lett. 2020, 11, 3515−3520